Volume and Surface Area Distributions of Cracks in Concrete

G. Nagy[1], T. Zhang[1], W.R. Franklin[1], E. Landis[2], E. Nagy[2], and D. Keane[3]

[1] Rensselaer Polytechnic Institute, Troy, NY, USA
[2] University of Maine, Orono, ME, USA
[3] Northwestern University, Evanston, IL, USA

Abstract. Volumetric images of small mortar samples under load are acquired by X-ray microtomography. The images are binarized at many different threshold values, and over a million connected components are extracted at each threshold with a new, space and time efficient program. The rapid increase in the volume and surface area of the foreground components (cracks and air holes) is explained in terms of a simple model of digitization. Analysis of the data indicates that the foreground consists of thin, convoluted manifolds with a complex network topology, and that the crack surface area, whose increase with strain must correspond to the external work, is higher than expected.

1 Objectives and Scope of the Paper

Many attempts to model or recognize shape and form are based on a bi-level representation of relatively simple objects. In contrast, we are faced with an engineering problem characterized by sequences of large, complex, volumetric gray-scale images. This data was produced by a unique imaging instrument designed for observing the internal structure of dense, heterogeneous materials. The resulting measurements will ultimately be used in multiscale modeling of the microstructure for improved understanding of the macroscopic mechanical properties of concrete [1–4]. So far we can report only some observations from which we attempt to deduce aggregate and individual shape properties of a large collection of objects and to separate material properties from image processing artifacts. Our work raises far more questions than it answers. We present it here in the hope of gaining assistance from the segment of the image processing community dedicated to allied pursuits.

More specifically, we propose to analyze thin, warped, interconnected volumetric entities in sequences of density images of samples of mortar. The data is obtained by high-resolution 3-D microtomographic imaging using an X-ray imager at the National Synchrotron Light Source at Brookhaven[5–7]. The images show crack formation in mortar and concrete under increasing strain. Other applications with similar filiform and quasi-manifold configurations are membranes, plant and animal vasculature, nerve fibers, and polymers, all of which can be imaged through soft-tissue tomography, magnetic resonance imaging, 3-D ultrasound, or confocal microscopy. The topological complexity of such data precludes 2-D analysis.

The detection, quantification and further analysis of structural changes in cement-based materials offers the potential for a more rational approach to the design,

testing, repair, or replacement of concrete structures. The total replacement value of concrete structures in the US has been estimated to be over six trillion dollars. While continuum approaches based on plasticity and linear elastic fracture mechanics have led to considerable success in predicting failure in fine-grained materials such as metals, non-linear effects have resisted analysis in heterogeneous and quasi-brittle materials such as concrete. The study of microstructure coupled with traditional stress-strain measurements offers the most promising approach [8–10]. In concrete, cracks are thought to originate from one or more porous voids, and they may even spread preferentially through voids and pre-existing cracks. We hope that the detailed mechanisms of crack origination and propagation may be revealed by 3-D X-ray imaging.

2 Data Collection

Microtomography yields a 3-D map of absorptivity from hundreds of through-transmission radiographs of the specimen taken from different angles. It is similar to medical CAT scans, except for much higher beam intensity and detector resolution. The specimen is rotated on a stage designed to allow the application of a load while minimizing X-ray absorption [11–13](Figure 1).

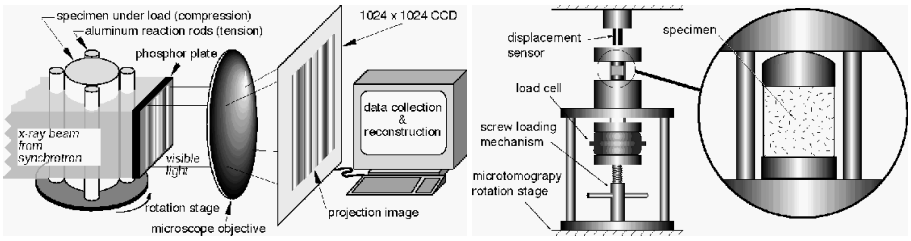

Fig. 1. (left) The system for x-ray microtomography; (right) the load cell for holding the composite material specimens under calibrated loads.

The specimens are small mortar cylinders under axial compressive load. The stress is continuously monitored by a conventional load cell, and the platen-to-platen displacement by a linear-voltage displacement microprobe. The data is collected and preprocessed by the University of Maine team at Beamline X2B. The X-ray source is synchrotron radiation with a highly collimated narrow-band beam monochromated to 32keV. The detector is a phosphor plate from which light is captured by a high-resolution CCD camera. The specimens are exposed to the beam at 720 different angles over a 180 degree range. Each exposure lasts 8-12 seconds, depending on the synchrotron beam current. This combination results in a very high resolution (2-6 μm) 3-D array, but the capture cross section is limited to about 6mm by the beam width.

The resulting data (Figure 2) consists of sequences of 3-D integer arrays representing localized X-ray absorption. The dimensions of each array, reconstructed

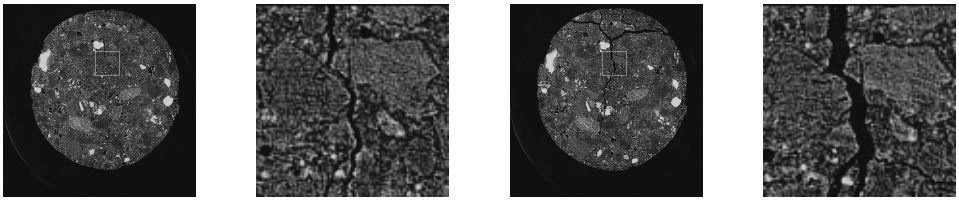

Fig. 2. Two 2-D circular slices of concrete, gray-scale, one each from successive loads, at corresponding heights. Enlargement of 100×100 squares across the large crack.

by the EXXON Direct Fourier Reconstruction algorithm on site, are typically $1024 \times 1024 \times 800$ voxels. A new array is generated from the specimen after each of 5 or 6 load-and-release cycles with progressively greater loads. The last image is intended to capture the state of the specimen after the peak of the stress-strain curve, when any further load would cause it to crumble. Each sample requires about 6 hours of "beam-time". The images are originally recorded as 32-bit floating-point numbers, and then scaled to eight bit integers. In our representation, high gray values (shown as white or light gray) indicate high X-ray absorption, and low values (shown as dark gray or black) indicate voids consisting of cracks and air holes. When the data is binarized to 0-1, a higher threshold increases the number of foreground (black, i.e., 0) voxels.

3 Methods and Observations

The surroundings of the sample concrete cylinder are transparent to X-rays just as are the voids inside the cylinder. However, many cracks reach the external surface. In order to apply connected-components analysis, it is necessary to separate the exterior volume from the crack volume. This is accomplished by "shrink-wrapping" the cylinder. The resulting cross-sections are neither truly circular nor convex, and change along the axis.

Our 3-D processing relies heavily on connected components (CC) analysis [14–16]. We have developed and tested a robust algorithm that is space- and time-efficient because it is implemented as a Find-Union on 1-D runs, with path compression. In a test array of size $800 \times 800 \times 765$ (489,600,000 voxels), it finds six million six-connected components in 200 seconds (400 MHz Pentium with 640Mbytes of RAM). In addition to listing all of the connected components with their constituent voxels, the program reports the volume, surface area (number of free faces) and the number of foreground runs in each CC. The code and test cases are freely available on `http://www.ecse.rpi.edu/Homepages/wrf/research/connect/`.

We use VTK, the 3D Visualization Toolkit, to visualize the cracks. VTK is an open source, surface-based rendering software system from kitware.com. Its rendering support is based on triangulating the gray-scale isosurfaces using Marching Cubes [17, 18]. Other routines were developed to analyze the volume distribution, free surface histograms and merge graph of the connected components.

The remainder of the paper presents the observations in detail and attempts to explain them in terms of the characteristics of the sample and of a simple model of the digitization process.

3.1 Effects of Amplitude Quantization

The radiographic quality of the image data is quite consistent. There is little variation in grayscale from sample to sample, because fluctuation in the electron beam intensity is compensated for by periodic recording of a blank picture (without the sample). The gray scale does not capture the full dynamic range. The high absorption regions of mortar have a uniform value of 255 and some cracks and voids are saturated at 0. Nevertheless, there is sufficient contrast to discriminate the structure.

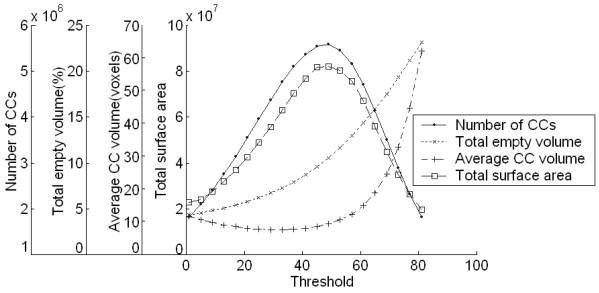

Fig. 3. Number of CCs, foreground (empty) volume, average CC volume, and surface area against binarization threshold for the whole shrink-wrapped volume of a sample.

The aggregate (larger particles) is even more opaque to X-rays than the mortar, while air is transparent. Given the high-contrast nature of the object under study, any threshold in a wide range should be equally satisfactory for isolating the voids (cracks and air holes). It turns out, however, that the choice of threshold has a very significant effect on the characteristics of the binarized image.

According to Figure 3, the total foreground volume increases gradually from 4% of the sample to 24%. The apparent crack-volume changes by a factor of more than three with threshold in the operational range of threshold from 40 to 60. This is a much larger change than that due to increased load at a constant threshold. It can be explained by the model of digitization presented below. At the same time, the number of CC's rises from nearly 1.8 million to nearly 5.5 million, then decreases to 1.8 million again. We conjecture (see below) that at the lower thresholds only thick voids are revealed. The eventual drop is expected: if the threshold is raised above the value of all voxels, then the entire sample will consist of a single connected component. Figure 4 shows representative 2-D cross sections at two thresholds at successive loads.

Because the work performed by the external force is expected to equal the work required to stretch the internal surfaces, the crack surface area is an important parameter. Furthermore, the ratio A/V of surface area to volume (akin to perimeter/area in 2-D) is a useful measure of rotundity that may separate cracks from air holes. The ratio $A^{\frac{3}{2}}/V$ is a *shape invariant*.

The Area/Volume ratio of the largest CC in a $200\times200\times200$ block (Figure 5) falls as expected to a threshold of 40, then rises as even thinner and more tortuous cracks are merged to it. The maximum Area/Volume ratio is only 2.5.

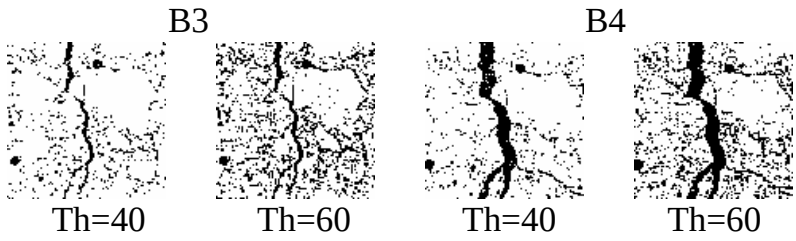

Fig. 4. 2-D bilevel X-section at thresholds of 40 and 60 at successive loads.

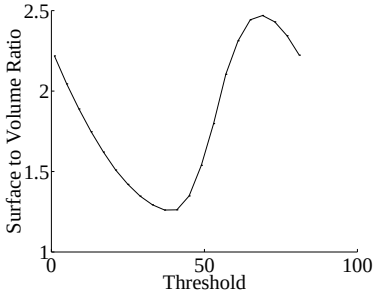

Fig. 5. Surface area to volume ratio of the largest CC in a 200×200×200 voxel block.

	Cube	One-voxel thick slab
Free face	Voxel Number	Voxel Number
0	5832	0
1	1944	0
2	216	7744
3	8	352
4	0	4
Total	8000	8100

Fig. 6. Free surface distribution

In compact objects, most of the voxels would be either interior voxels, with no free face, or surface voxels with exactly one free face. The number of free faces is shown in Figure 6 for a 20×20×20 cube and a one-pixel thick 90×90 slab. In concrete, there are many voxels with several free surfaces, as seen in Figure 7, indicating highly irregular, tortuous surfaces. The skew increases with threshold, because although the larger CCs have more interior voxels, we are adding many smaller cracks.

The logarithmic scatter plots of Figure 7 show that the CCs range from flat or filiform (upper envelope: A/V constant) to filled-out shapes (lower envelope: $A^{\frac{3}{2}}/V$ constant). The larger the components, the thinner they are.

3.2 Effects of Spatial Quantization

Because of the presence of so much boundary surface (between foreground and background), reducing the resolution by subsampling by 8 the data has a very different effect from averaging it over 2×2×2 volumes. Figure 8 compares histograms resulting from subsampling and interpolation. This result indicates that we can expect radically different results as the resolution of the imager is enhanced.

3.3 Crack Size and Connectivity

Figure 9 shows that the distribution of crack size is qualitatively similar at different thresholds. About half of the CCs are smaller than 1000 voxels, while the largest CC

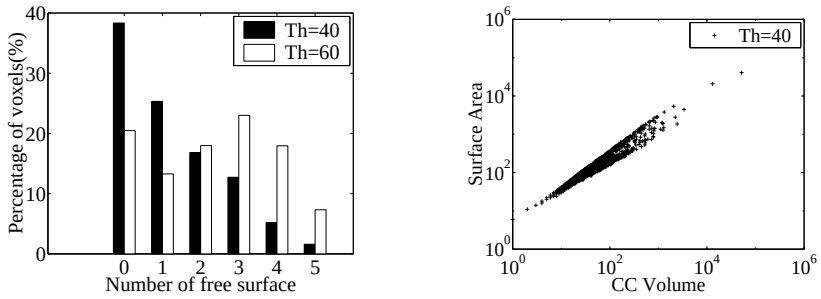

Fig. 7. (left) Bar chart of distribution of free faces at two thresholds; (right) scatter plot of surface area vs. CC volume at two thresholds.

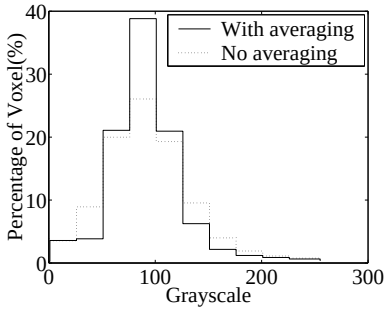

Fig. 8. Grayscale histogram of reduced samples.

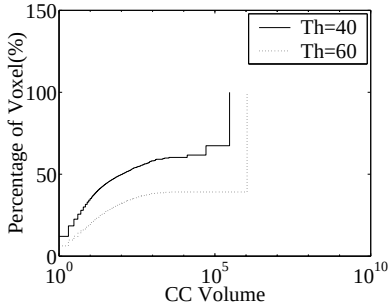

Fig. 9. The empty voxel distribution versus CC volume of a 200×200×200 voxel block.

accounts for one third to one half of the total foreground volume. The CCs span six orders of magnitude in size.

The presence of a huge number of tiny foreground CCs at any threshold is certainly suggestive of noise, but may also be a property of the material. We will soon obtain multiple images of the same sample to resolve this question. We have also noted patterns of horizontal circular caused by the reconstruction of irregularities in the phosphor or spread of the X-ray beam.

It is possible to trace the merging of the largest components as the threshold changes (Figure 10). Each merger results in an abrupt increase in the volume and surface area of the resulting composite CC. The mergers are caused by the emergence of thin ”bridge” cracks as the threshold is increased. A complete merge graph has millions of nodes. Ultimately we are interested in tracing the merger of cracks with increasing load.

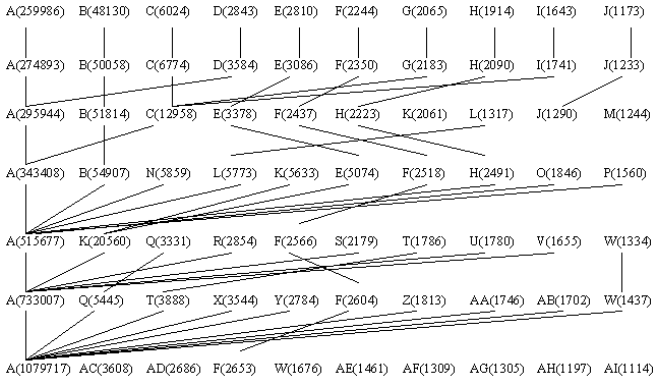

Fig. 10. Merge graph of the largest cracks(the numbers being the volume of cracks).

3.4 Point Spread Function

Most of the above observations can be explained using a simple model of digitization. We present the model in one dimension in order to be able to graph the functions. In the model, the cracks have a constant (one) density. The width of the cracks is distributed exponentially. The space between cracks is also distributed exponentially. The point spread function is modeled with a Gaussian. The ‘analog’ crack signal is convolved with the Gaussian, then thresholded and sampled. (The relative order of thresholding and sampling is immaterial.) The left of Figure 11 shows the original crack distribution, the convolved signal, and the binarized distribution at two different thresholds. As the threshold is decreased, nearby cracks are merged and new, thinner cracks appear. The width of the point spread function is more than 2 voxel diameters, as indicated by the cross section of cracks in the right of Figure 11.

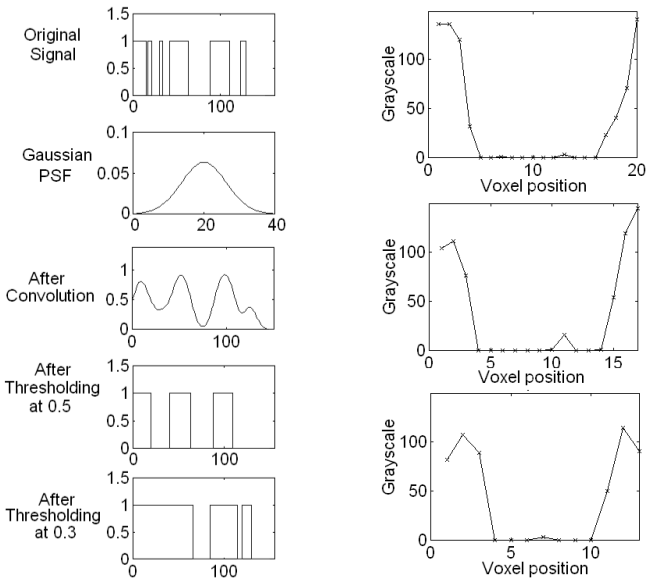

Fig. 11. (left) Model of Digitization; (right) sample profiles of grayscale across larger cracks.

4 Discussion

The samples consist of a huge number of very thin cracks, and a few wide cracks. The entire volume, except for the aggregate, appears to be traversed by cracks (*craquelure*). It is possible that most of these cracks are connected, but the point-spread function of the imager is too large to yield convincing proof.

A fast CC program is essential for studying the image at a wide range of threshold settings because the large point-spread function of the imaging system, compared to the spatial sampling interval, obscures the intrinsically high contrast between mortar and voids. This also accounts for the rapid growth in the volume of black pixels as the threshold is increased. For now, we can only speculate whether the point-spread function is dominated by the phosphor or the granularity of the reconstruction algorithm (the cooled CCD camera is not a likely culprit).

The thin cracks have very convoluted boundaries, which result in a high surface-area to volume ratio. Therefore, visualization software yields very little insight into the structure, and a quantitative approach is required. With increasing threshold, the number of boundary voxels increases faster than the number of interior voxels, resulting in an overall increase in the surface-area to volume ratio. The results on subsampling indicate that the current spatial sampling resolution is insufficient to give a true measure of the (possibly fractal) surface area of the crack boundaries. Such a measure is necessary to compare the increase in total crack surface area from load to load with theoretical predictions based on the loading and relaxation stress-strain curves. Although the resolution of the X-ray beam and of the optical system allows us to increase linear resolution by at least a factor of four (at the cost of a 64-fold increase in acquisition

time and data volume, and a corresponding decrease in sample volume), electron micrographs would be useful here.

Under load, the volume of the largest connected components grows more quickly than the total volume of black pixels, as observed at any threshold. Equivalently, as the load increases, the volume of small connected components relative to the total black volume decreases because their expansion under load results in the small cracks being connected to the larger cracks. This effect is superficially similar to apparent crack growth with increasing threshold.

5 Future Work

We have much work ahead of us. We don't yet have any effective measures of crack shape and crack topology. Before modeling crack propagation under load, it will be necessary to model both the cracks and the density variations in the material itself. Furthermore, current 3-D image registration techniques will have to be extended to the compound problem of bringing into correspondence objects exhibiting both global distortion (motion of the sample) and local changes due to crack growth. After separating cracks from noise specks and air holes on the basis of volume and surface area, we can verify that cracks grow from load to load, air holes remain the same, and noise specks appear and disappear randomly.

Another important issue is the pore structure connectivity that governs water penetration from the surface. From the CC analysis we can determine which cracks open to the surface. By tracing these cracks, we can compute what fraction of the volume is a given distance from the surface. The change of permeability with crack growth affects long-term durability of concrete. An open question is the rate at which hairline cracks merge to form macro-cracks under load. Our long-term goal is the parameterization of crack growth for multiscale finite element modeling and analysis.

References

1. J.G.M. van Mier, Fracture Processes of Concrete, CRC Press, New York, 1997.
2. Z.P. Bazant, Analysis of Work-of-Fracture Method for Measuring Fracture Energy of Concrete. Journal of Engineering Mechanics, **122**(2), 138-144, 1996.
3. S.P. Shah, ed., Toughening mechanisms in quasi-brittle materials, Kluwer-Academic, Dordrcht 1990.
4. S.P. Shah, S.E. Swartz, C. Ouyang, Fracture mechanics of concrete: applications of fracture mechanics to concrete, rock, and other quasi-brittle materials, Wiley, New York, (1995).
5. F.O.Slate, S.Olsefski, X-ray study of internal structure and microcracking of concrete, J.Am. ConcreteInst.60,5,pp.575-588,1963
6. Flannery, B. P., Deckman, H. W., Roberge, W. G., and D'Amico, K. L. (1987) Three-Dimensional X-ray Microtomography. Science, **237**, 1439-1444.
7. H. W. Deckman, J. H. Dunsmuir, K.L. D'Amico, S.R. Ferguson, B.P. Flannery, Development of Quantitative X-ray Microtomography. Materials Research Society Symposium Proceedings, **217**, 97-110, 1991.
8. E. N. Landis, E. N. Nagy, D. T. Keane and N. Huynh, Observations of Internal Fracture in Mortar using X-Ray Microtomography, Proceedings of the ASCE Engineering Mechanics Specialty Conference, Ft. Lauderdale, FL, May, 637-640, 1996.

9. E. N. Landis, E. N. Nagy, D. T. Keane and S. P. Shah, Observations of Internal Crack Growth in Mortar using X-ray Microtomography, in Proceedings of the 2nd International Conference on Nondestructive Testing of Concrete in the Infrastructure, June 12-14, Nashville, TN, Society for Experimental Mechanics, 54-59, 1996.
10. E. N. Landis, E. N. Nagy and D. T. Keane, Microtomographic Measurements of Internal Damage in Portland Cement-Based Composites, Journal of Aerospace Engineering, V. 10, No. 1, 2-6, 1997.
11. E. N. Nagy and E. N. Landis, Analysis of Microtomographic Images to Measure Work of Fracture in Concrete, in Review of Progress in Quantitative Nondestructive Evaluation 16, D. O. Thompson and D. E. Chimenti, Eds., Plenum Press, New York, 1761-1766, 1997.
12. E. N. Nagy and E. N. Landis, Energy-Microcrack Growth Measurements for Mortar Cylinders in Compression, in Nondestructive Characterization of Materials in Aging Systems, R. Crane, Eds., Materials Research Society, 1998.
13. E.N. Landis, E.N. Nagy, D.T. Keane, G. Nagy, A technique to measure three-dimensional work-of-fracture in concrete, Journal of Engineering Mechanics 126, 6, pp. 599-605, June 1999.
14. C. Ronse and P.A. Devijver, Connected components in binary images: the detection problem, Research Studies Press, Letchworth, England, 1984.
15. H. Samet, Applications of Spatial Data Structures, Addison-Wesley 1989.
16. G. Borgefors, I. Nystrom, G. Sanniti de Baja, Connected components in 3D neighborhoods, Procs. 10th Scandinavian Conf. on Image Analysis (SCIA'97), 557-570, Helsinki 1997.
17. W.J. Schroeder, Geometric triangulation with application to fully 3-D automatic mesh generation. PHD dissertation, Rensselaer Polytechnic Institute, Troy, NY May 1991.
18. L.L. Schumaker, Triangulations in CAGD, IEEE Computer Graphics and Applications 13, 1, 47-52, 1993.